Absolute cryogenic radiometer for high accuracy optical radiant power measurement in a wide spectral range

Haiyong Gan (甘海勇)*, **Yingwei He** (赫英威), **Xiangliang Liu** (刘想靓), **Nan Xu** (徐 楠),
Houping Wu (吴厚平), **Guojin Feng** (冯国进), **Wende Liu** (刘文德),
and **Yandong Lin** (林延东)

Division of Optics, National Institute of Metrology, Beijing 100029, China
*Corresponding author: ganhaiyong@nim.ac.cn
Received March 30, 2019; accepted May 23, 2019; posted online July 24, 2019

An absolute cryogenic radiometer (ACR) with a detachable optical window was designed and built for high accuracy optical radiant power measurement and photodetector spectral responsivity calibration. The ACR receiver is an electroplated pure copper cavity with a 50-μm-thick wall and inner surface coated with a specular black polymer material mixed with highly dispersible carbon nanotubes. The absorptivity of the cavity receivers was evaluated to be ≥0.9999 in the 250 nm–16 μm wavelength range and ≥0.99995 in 500 nm–16 μm. The cavity receiver works at the temperature of ~5.2 K with nanowatt-level noise-equivalent power. The relative standard uncertainty is 0.041% for the measurement of ~100 μW optical radiant power (250 nm–16 μm) and 0.015% for ~1 mW (500 nm–16 μm).

Absolute electrical substitution radiometers (ESRs) working at cryogenic temperatures were first developed at the National Physical Laboratory (NPL) in the UK with superior performance to those working at ambient temperature[1], owing to the following major accomplishments: (1) the thermal noise from low temperature background decreases dramatically; (2) the specific heat of pure copper at low temperature reduces by a few orders so the cavity receiver made from electroplated high purity copper can be significantly more sensitive to heat; and (3) the thermal conductivity of pure copper at low temperature increases by several times so the non-equivalence between the electrical and optical heating on the cavity receiver can be less influential.

Works on high accuracy measurement of optical radiant power based on absolute cryogenic radiometers (ACRs) have been conducted worldwide[2–7]. The ACRs have also been spontaneously adopted as laboratory irradiance standards, remote sensing detectors, and pyrheliometers based on the abundant experience on finely studied ambient-temperature ESRs[3,8]. Thanks to their unmatched measurement uncertainties, ACRs have been well recognized as a primary detector for the realization of candela and associated derived units for photometric and radiometric quantities in the International System of Units (SI)[9].

ACRs have played a critical role in metrology and drawn increasing amounts of interest from important applications fields such as earth observing systems (EOS). For instance, scientists from the National Institute of Standards and Technology (NIST) in the U.S. successfully applied the ACRs for the low background infrared (LBIR) measurement facility and effectively provided traceability to the calibration of remote sensing instruments for missile defense and climate research[10]; scientists from the NPL

and their global research partners initiated an ambitious plan for traceable radiometry underpinning terrestrial- and helio-studies (TRUTHS) in order to satisfy the low uncertainty calibration demands for the cutting-edge EOS sensors and technologies[11]. The application scopes of ACRs would be further broadened, especially when mechanically cooled ACRs with simplified handling and sustainable operability were invented, and the specifications were determined to be comparable to those cooled by liquid helium[12,13].

Chinese scientists have been actively working on ACRs for more than twenty years and made important progress on ACR component renovation, spectral range extension, quality calibration service, and system development[14–19].

Herein, we report our recent achievement of building a home-made ACR for a wide spectral range, high accuracy optical radiant power measurement with a standard uncertainty of 0.041% at the ~100 μW level in the 250 nm–16 μm range and 0.015% at the ~1 mW level in the 500 nm–16 μm range.

The ACR was designed as illustrated in Fig. 1 with a detachable wedged optical window between the power-stabilized laser system and the ACR main chamber. The power-stabilized laser system was integrated on a small platform with an area of about 0.6 m × 0.9 m (as shown in Fig. 2) and mounted on a cart with good mobility. After laser power measurement, a vacuum valve on the ACR main chamber was closed, the power-stabilized laser system was detached off the ACR main chamber, and the optical window was part of the power-stabilized laser system without significant relative position change. Hence, the optical radiant power measured by the ACR can be directly delivered onto a photodetector under test for spectral responsivity calibration with no need to worry
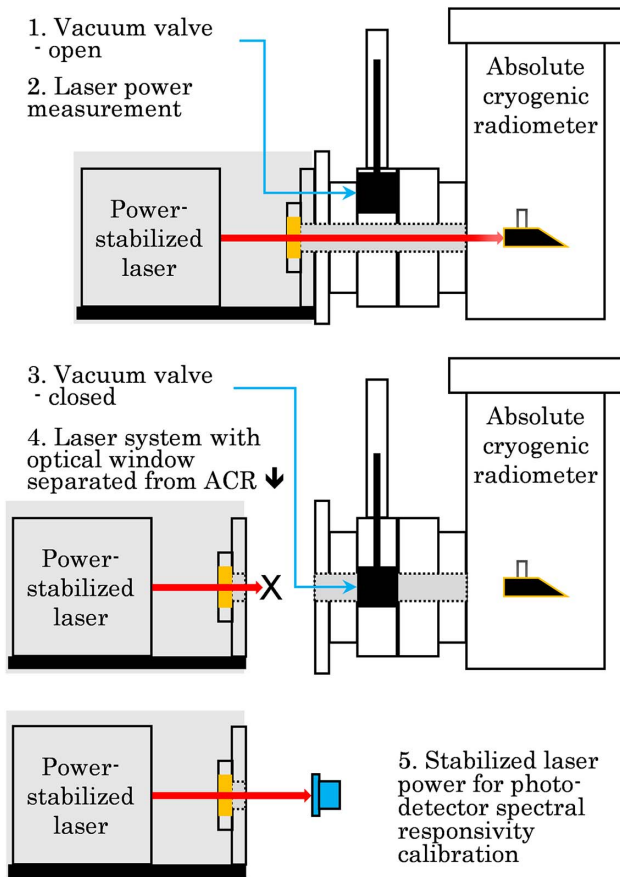
Fig. 1. Optical radiant power measurement and photodetector spectral responsivity calibration scheme.
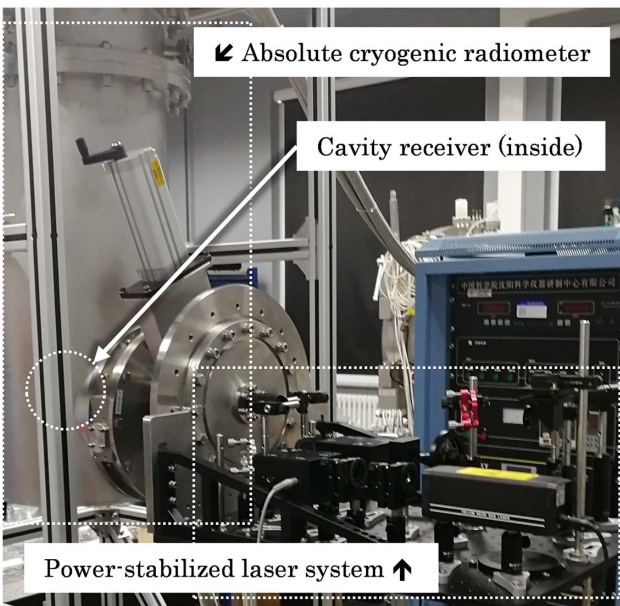

Fig. 2. ACR facility at the National Institute of Metrology, China.

about the transmittance of the optical window (e.g., ~94% at 633 nm for a 10-mm-thick uncoated UV fused silica window). The ACR facility is shown in Fig. 2.
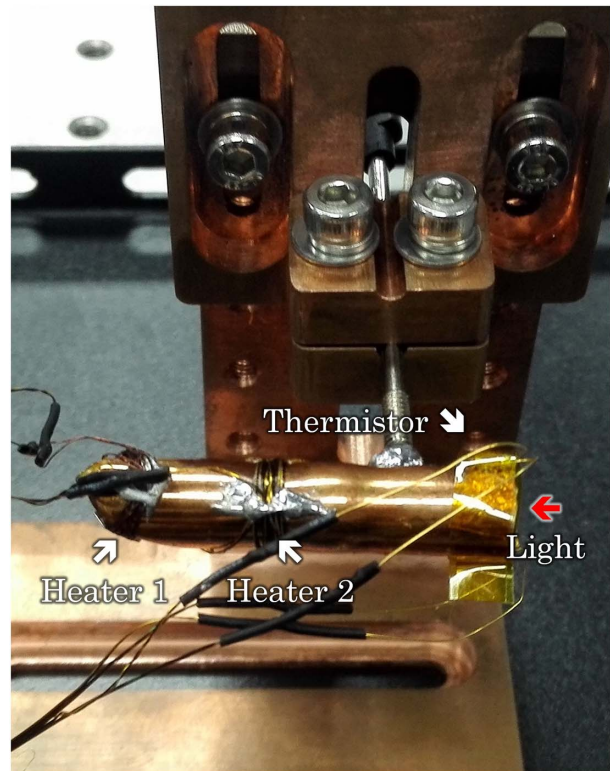

Fig. 3. Picture of the ACR cavity receiver.

The cavity receiver of the ACR has a classical tube shape (Fig. 3) with a 30 deg slanted bottom made by the electroplating method. The full length is around 40 mm, the diameter of the open end is 10 mm, the wall thickness is 0.05 mm, and the total weight is less than 1 g. A polyurethane-based material blended with highly dispersible acidified multi-walled carbon nanotubes was applied to coat the inner surface of the cavity receiver for high absorptivity. The spectral diffuse reflectance of the coating material on a flat substrate was measured over 250 nm–2500 nm with the specular component excluded and over 250 nm–16 μm with the specular component included, respectively (Fig. 4). The absorptivity of the coated cavity receiver was measured to be 0.99995 at the wavelength of 1.55 μm using the laser-based diffuse reflectance method. Due to the flatness of the spectral diffuse reflectance shown in Fig. 4, the absorptivity of the coated cavity receiver can be extrapolated to be no less than 0.9999 in the 250 nm–16 μm spectral range and 0.99995 in 500 nm–16 μm.

A highly sensitive low temperature thermistor was placed on the cavity wall near the open end to measure the temperature change induced by either electrical or optical heating. Two 10 K ohm heaters were mounted on the slanted bottom surface separated by a distance of 10 mm and lined up with the thermistor. About 1 mW of the same electrical power was applied on each heater in turn to measure the temperature change difference and, hence, the cavity thermal non-equivalence to be no higher than 0.005%.
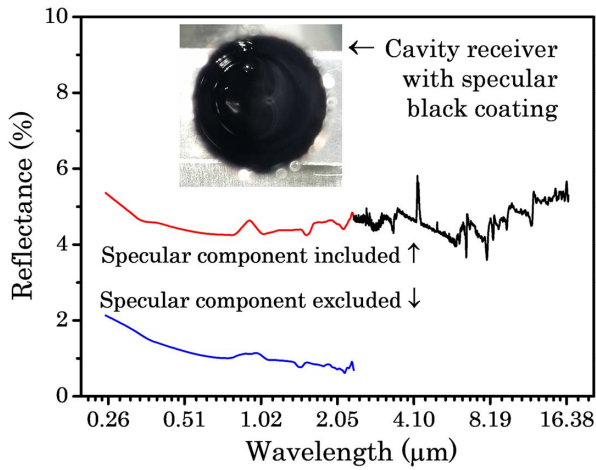
Fig. 4. Spectral diffuse reflectance measurement results of the specular black material on a flat surface. Inset: the cavity receiver with the inner surface coated with the specular black material.

The cavity receiver was then installed on a base, and then a sample stage was connected to the second stage cool head of a Gifford–McMahon-type mechanical cryocooler (Pride Cryogenics, China) with a 1.5 W cooling power at 4.2 K. The temperature of the sample stage is actively controlled at 5.2 K. A stainless-steel rod was adopted as the thermal link between the cavity receiver and its base. The thermal impulse response time constant of the cavity receiver is about a few tens of seconds, and the optimal work time for complete thermal equilibrium is approximately several minutes.

Normally, the heat sensitivity of the cavity receiver can be higher when a weaker thermal link is used, although the thermal impulse response time constant becomes larger and consequently requires a longer period of system thermal stability. In our work, the ACR background temperature can be well controlled for 7 min with a noise-equivalent power of a few nanowatts using the proportion-integral-differentiative method. However, unfavorable influence may occur during minutes-long complete equilibrium working time and compromise the measurements. Two different sets of means can be sought to solve this problem. The first set includes physical modification methods to lower the thermal impulse response time constant, such as (1) reducing the heat capacitance of the cavity receiver by revising the cavity size or wall thickness or so, and (2) increasing the thermal conductivity of the thermal link by changing the link material or the link diameter or so. The second set includes a series of actions based on heat transfer models and mathematical analyses to accelerate the measurement processes: first, experiment data were recorded for some time after heat switching but not until achieving complete thermal equilibrium; then, the first order derivatives of the thermistor resistance change were calculated, and the measurement data were re-aligned based on the first order derivatives correspondingly; and last, the thermistor resistance change

results at complete thermal equilibrium can be extrapolated when the first derivatives approach zero. In our work, the cavity receiver was designed to measure an optical radiant power as low as ~1 μW with high accuracy, and therefore, we took advantage of the mathematical methods to shorten the total work time instead of physically reducing the thermal impulse response time.

The thermistor resistance change (ΔR) data were recorded and shown in Fig. 5 for five rounds of heating and thermal recovery processes. The vertical axis is the resistance change, and the horizontal axis is the number of readings (N) with 0.5 s apart. It is worthy to note that none of the five rounds was fully settled to the complete equilibrium status, and the total work time can be estimated as having been reduced by half. The first order differentiative of the thermistor resistance change was calculated and plotted as in Fig. 6. Ideally, the thermistor
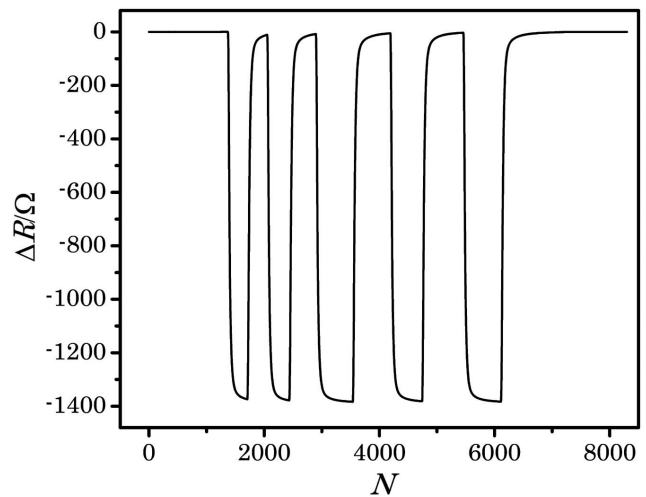

Fig. 5. Cavity receiver thermistor resistance records during the optical radiant power measurements without reaching full thermal equilibrium.
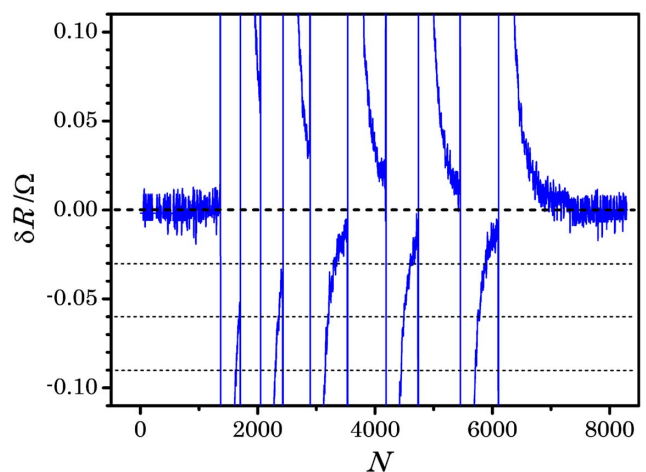

Fig. 6. Thermistor resistance reading changing rate during the optical radiant power measurements without reaching complete thermal equilibrium.

resistance change rate (the first order derivative, δR) at a certain resistance point should be proportional to the difference between that resistance and the equilibrium resistance. However, the actual situation may deviate dramatically from simple heat dissipation models. The thermistor resistance change rate was plotted against the corresponding resistance, and the relationship was illustrated in Fig. 7. When the thermistor resistance change rate goes down to near zero, the thermistor resistance converges to (-1384.9 ± 0.4) Ω, and the relative uncertainty of the repeatability for multiple rounds of measurements is 0.033%.

A He–Ne laser with 632.8 nm wavelength was vertically polarized and then stabilized with $\leq$50 ppm (parts per million) drifting by using a liquid crystal modulator. The effective electric heating power across the heater resistance was controlled at a 210 ppm relative uncertainty level. Since the electrical substitution can be performed with small intervals in power, the nonlinearity of the ACR can be minimized to negligible. The typical uncertainty source from the Brewster window is no longer an issue in this work due to the application of the detachable window on the ACR. The uncertainty for optical radiant power measurements using the home-made ACR can be evaluated to be 0.041% ($k = 1$) based on the analyses of the contributions from relevant sources, as listed in Table 1.

For optical radiant power measurement at the $\sim$1 mW level, the relative uncertainties of relevant sources are reduced significantly, such as the effective electric heating power and repeatability. If only the spectral range of 500 nm–16 µm is considered, the cavity absorptivity is higher than 0.99995, and the relative uncertainty is 0.005%. The relative uncertainty of the repeatability for multiple rounds of measurements is 0.01%. The combined relative standard uncertainty can then be evaluated to be 0.015% based on the uncertainty analyses highlighted in Table 2. The high accuracy absolute optical radiant

Table 1. Uncertainty Analysis for Optical Radiant Power Measurements at $\sim$100 µW (250 nm–16 µm)

Source	Type	Value (%)
Effective electric heating power	B	0.021
Cavity thermal non-equivalence	B	0.005
Cavity absorptivity (250 nm–16 µm)	B	0.01
Laser power stability	B	0.005
Nonlinearity	B	(–)
Repeatability	A	0.033
Combined uncertainty ($k = 1$)		0.041

Table 2. Uncertainty Analysis for Optical Radiant Power Measurements at $\sim$1 mW (500 nm–16 µm)

Source	Type	Value (%)
Effective electric heating power	B	0.007
Cavity thermal non-equivalence	B	0.005
Cavity absorptivity (500 nm–16 µm)	B	0.005
Laser power stability	B	0.005
Nonlinearity	B	(–)
Repeatability	A	0.01
Combined uncertainty ($k = 1$)		0.015

power measurement capability extended into the mid-infrared (MIR, including mid-wave infrared and long-wave infrared) wavelength range is important to provide effective traceability for the calibration of the laser power of MIR lasers, the spectral responsivity of MIR detectors, and the radiometric characteristics of MIR spectroradiometers[20,21].
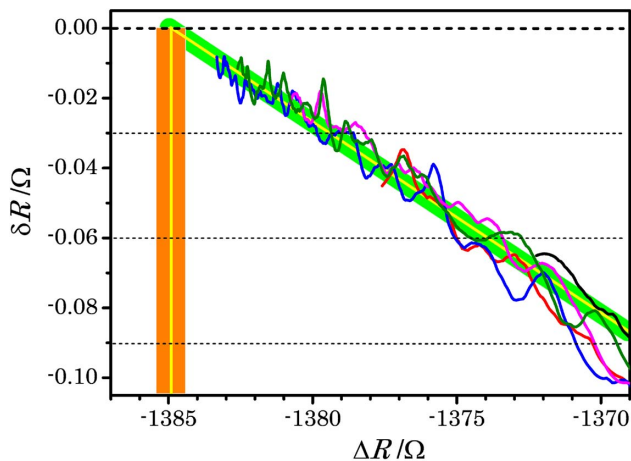
Fig. 7. Derivation of thermistor resistance at complete thermal equilibrium based on the optical radiant power measurement results without reaching complete thermal equilibrium.

References
1. J. E. Martin, N. P. Fox, and P. J. Key, Metrologia **21**, 147 (1985).
2. T. Varpula, H. Seppä, and J. M. Saari, IEEE Trans. Instrum. Meas. **38**, 558 (1989).
3. P. V. Foukal, C. Hoyt, H. Kochling, and P. Miller, Appl. Opt. **29**, 988 (1990).
4. R. U. Datla, K. Stock, A. C. Parr, C. C. Hoyt, P. J. Miller, and P. V. Foukal, Appl. Opt. **31**, 7219 (1992).
5. T. R. Gentile, J. M. Houston, J. E. Hardis, C. L. Cromer, and A. C. Parr, Appl. Opt. **35**, 1056 (1996).
6. K. D. Stock and H. Hofer, Metrologia **30**, 291 (1993).
7. S. P. Morozova, V. A. Konovodchenko, V. I. Sapritsky, B. E. Lisiansky, P. A. Morozov, U. A. Melenevsky, and A. G. Petic, Metrologia **32**, 557 (1995/96).
8. J. E. Martin and N. P. Fox, Metrologia **30**, 305 (1993).

9. J. Zwinkels, A. Sperling, T. Goodman, J. C. Acosta, Y. Ohno, M. L. Rastello, M. Stock, and E. Woolliams, Metrologia **53**, G1 (2016).

10. A. C. Carter, S. R. Lorentz, T. M. Jung, and R. U. Datla, Appl. Opt. **44**, 871 (2005).

11. N. Fox, J. Aiken, J. J. Barnett, X. Briottet, R. Carvell, C. Frohlich, S. B. Groom, O. Hagolle, J. D. Haigh, H. H. Kieffer, J. Lean, D. B. Pollock, T. Quinn, M. C. W. Sandford, M. Schaepman, K. P. Shine, W. K. Schmutz, P. M. Teillet, K. J. Thome, M. M. Verstraete, and E. Zalewski, Adv. Space Res. **32**, 2253 (2003).

12. N. P. Fox, P. R. Haycocks, J. E. Martin, and I. Ul-Haq, Metrologia **32**, 581 (1995).

13. K. D. Stock, H. Hofer, M. White, and N. P. Fox, Metrologia **37**, 437 (2000).

14. W. Pang, X. Zheng, J. Li, X. Shi, H. Wu, M. Xia, D. Gao, J. Shi, T. Qi, and Q. Kang, Chin. Opt. Lett. **13**, 051201 (2015).

15. K. Zhao, X. Shi, H. Chen, Y. Liu, C. Liu, K. Chen, L. Li, H. Gan, and C. Ma, Metrologia **53**, 981 (2016).

16. N. Xu, Y. Lin, H. Gan, and J. Li, Proc. SPIE **10155**, 1015513 (2016).

17. X. Zhao, Y. Zhao, K. Tang, L. Zheng, S. Liu, Y. Zhao, F. Li, and M. Cui, Nucl. Tech. **41**, 040101 (2018).

18. X. Ye, X. Yi, W. Fang, K. Wang, Y. Luo, Z. Xia, and Y. Wang, IET Sci. Meas. Technol. **12**, 994 (2018).

19. X. Zhuang, H. Liu, P. Zhang, X. Shi, C. Liu, H. Liu, and H. Wang, Acta Phys. Sin. **68**, 060601 (2019).

20. Z. Qin, G. Xie, J. Ma, P. Yuan, and L. Qian, Chin. Opt. Lett. **15**, 111402 (2017).

21. J. Hua, Z. Wang, J. Duan, L. Li, C. Zhang, X. Wu, Q. Fan, R. Chen, X. Sun, L. Zhao, Q. Guo, L. Ding, L. Sun, C. Han, X. Li, N. Wang, H. Gong, X. Hu, Q. Liao, D. Liu, T. Yu, Y. Wu, E. Liu, and Z. Zeng, Chin. Opt. Lett. **16**, 111203 (2018).